

ALMA Memo No. 320

Strawperson Donut/Doubling-Ring Configurations

M. S. Yun & L. Kogan
National Radio Astronomy Observatory

August 24, 2000

Abstract

1 Introduction

The main motivation for the ALMA configuration design is delivering the best imaging performance possible given its number of antennas and the site limitations. The sensitivity and resolution requirements are driven by the scientific needs. Fourier plane coverage and the inclusion of short spacing information will dictate whether the target source brightness distribution can be faithfully recovered.

There are also practical concerns such as the array construction and operation costs. The cost of building antenna pads, cabling, and service roads is a substantial fraction of the total project budget (reference costing documents), and maximum sharing of the pads is one of the practical goals for the array design. Operational issues such as the ease and speed of reconfiguration also have an impact on the long term cost of the array (see Holdaway 1998a, Yun & Kogan 1999, Guilloteau 1999).

In this memo, we present a set of strawperson configurations for ALMA based on a “donut” or “double-ring” layout that are capable of addressing a number of these scientific and operational concerns. There are significant motivational and operational differences between our strawperson concept and the spiral zoom array concept proposed by Conway (2000a,b) as described below.

2 Design Motivations

2.1 Donut/Double-Ring Design

A circular ring is a classic array design with a number of desirable and undesirable qualities. For a relatively large numbers of elements N , a ring array can produce a uniform sampling of the uv-plane, much the same way a Reuleaux triangle can (Keto 1997), and Woody (1999) proposed a design concept with complete uv-coverage based on a ring layout. A ring array of diameter D with N elements also has abundant short baselines of length $\pi D/N$, providing an excellent spatial dynamic range for an array of size D . A classic problem with a ring array, however, is the large near-in sidelobes resulting from a nearly uniform radial distribution of the weights and a truncation at radius D – i.e. Fourier Transform of a circular aperture.

The “offset concentric” array seen in the artist’s conception of the old MMA has its roots in the MMA Memo 111 by Holdaway (1994), which describes a set of preliminary MMA configurations that can be accommodated on the limited real estate atop Mauna Kea. It should be noted that the main design emphasis was on the restrictions posed by the site, and relatively little consideration was given to the uv-coverage at the time.

Nevertheless there are significant merits to consider arrays consisting of nested rings. When we expand from a single ring to two concentric rings, the characteristic length scales diversify from two (D and $\pi D/N$) to six (D_1 , D_2 , $\pi D_1/N_1$, $\pi D_2/N_2$, $\frac{D_1-D_2}{2}$ and $\frac{D_1+D_2}{2}$). The net result is that the radial distribution of the weights becomes much more tapered, and the classic problem of the large near-in sidelobe can be significantly reduced. To mention briefly, the main impact of an offset concentric layout is breaking the radial symmetry and creating an axial symmetry instead, resulting in an elongated synthesis beam (N-S elongation for a displacement in E-W direction).

2.2 Kogan Optimization

Another important ingredient in designing our strawperson array concept is the implementation of the sidelobe minimization algorithm by Kogan (1998a). Even with the diversification of length scales resulting from having two rings, the residual discreteness in the radial distribution, also known as “wedding cake” effect, can produce radial sidelobes that may adversely

affect the deconvolution performance. Also, the periodicity resulting from a uniform distribution of elements along each ring can result in large azimuthal sidelobes. While the algorithm described by Kogan is not specifically designed to address these particular problems, the sidelobe minimization effectively breaks down any discrete structures and periodicity in both radial and tangential directions, smoothing out the harmful sidelobe structures and any discreteness in the radial distribution of the visibilities.

2.3 Other Considerations

Another significant underlying assumption is a VLA-like operation model with a discrete set of arrays, each designed for excellent imaging and self-similarity for matched resolution observations. There are both advantages and disadvantages to this operational model (see Yun & Kogan 1999, Guiloteau 1999, Conway 2000a), and several practical issues may ultimately determine the preferred operational mode. For example, limitations on the ease and speed of reconfiguration due to high wind may favor a more continuously reconfigurable array design. In contrast, reconfiguration in bursts is more robust against persistent adverse weather conditions lasting longer than a week or more.

The compact configuration is a filled array with 32 antennas located along a 150m diameter ring and the remaining 32 antennas densely filling the region inside. The four larger arrays are made up of four nested rings, each individual array consisting of two adjacent ring pairs. The scale factor of 2.1 between the inner and outer ring (and thus between the adjacent configurations) are determined by the ratio between the largest (3000m) and the smallest (150m) ring and the total number of desired resolution steps (5). Since each principal reconfiguration is accomplished by leap-frogging antennas on one ring over the next ring, a full reconfiguration can be accomplished by moving just 32 out of 64 antennas. All of the pads along the intermediate ring are thus re-used once, and the required total number of pads is $32 \times 4 + 64 = 192$.

All pad positions are chosen based on the 5 degree gradient digital topographical mask produced by B. Butler. The general area that can accommodate the largest (3 km) array within the Science Reserve boundary was located first, and the subsequent array and pad positions are found following the requirements discussed above.

While most observations should be made near transit, particularly at submm wavelengths (see Holdaway 1998b), designing in a N-S elongation

Table 1: Summary of ALMA strawperson configurations

Array	Minimum Baseline [m]	Maximum Baseline [m]	Time for FOC = 0.4 [hrs]	Natural Beam at 345 GHz [arcsec]
A	85	3000	10	0.050
B	35	1430	4	0.101
C	15	680	1.5	0.22
D	15	325	0.5	0.47
E	15	150	0.02	0.97

into all arrays is highly desirable in order to produce a more circular synthesize beam for a wide range of declination. A 10% N-S elongation for all arrays has been proposed by Helfer & Holdaway (1998), and it is implemented in our strawperson designs. Note that hybrid configurations with N-S elongation of 2:1 can also be easily accommodated by moving the first 16 antennas to the northern and southern pads in next largest ring.

3 Strawperson Configurations

The physical properties of the strawperson configurations are summarized in Table 1. The names of the arrays are assigned alphabetically from A to E, generally following the convention at the VLA, but they are otherwise completely arbitrary. Details of the individual configuration is discussed further below.

3.1 Compact Array (E-Array)

As stated already, the compact configuration is a filled array consisting of a 150m diameter ring of 32 antennas plus the remaining 32 antennas densely filling the inner circular region as shown in Figure 1. This array is optimized for high surface brightness sensitivity, and a “crystalline” array design was used as the initial point for the Kogan algorithm. To minimize the large sidelobes resulting from a filled array, the outer boundary of the array is pushed out to a diameter of 150m in order for the Kogan algorithm to

operate. This 150m diameter is chosen so that the synthesized beam at 345 GHz is about $1''$, matching the ground-based optical/IR imaging resolution even in this most densely packed configuration.

Another important motivation for the compact array is the instantaneous uv-coverage required for successful mosaic imaging. Most filled array should be able to meet this requirement naturally, and our design can sample nearly 50% of all uv cells instantaneously.

One other important design consideration unique to the compact array is the access to inner antennas. Many of the antennas shown in Figure 1 are packed close to the minimum distances of 15m, and a direct access to the antennas located inside the 150m diameter ring is not generally possible. The current design for the ALMA transporter has a width of 11m, and a transporter carrying an antenna can pass between two antennas if the two are separated by 18m and if both reflectors are facing away from each other. For an uninhibited access, the minimum distance between the antennas has to be larger than $7.5m + 12m + 7.5m = 27m$. Thus we designed in four “gates” with a width $\geq 27m$ along the outer ring in order to allow a direct access to a large number of the inner antennas. There are enough passages wider than 18m among the subsequent antennas so that the majority of the inner antennas can be reached without affecting too many other antennas. A small number of antennas are still very difficult to get to, and accessing some of the inner antennas may be best done by moving one outer ring antenna to a nearby temporary pad (built specifically for this purpose or one along the next ring). Drafting a detailed access plan for each of the antennas (for servicing or reconfiguration) is probably needed as part of the operational plan.

3.2 Intermediate Arrays

All arrays larger than the compact array are essentially self-similar in shape and scale up by factors of 2.1, each consisting of two nested rings and with 32 pads each. This arrangement allows a more centrally condensed uv-distribution compared with a single ring array, but the resolution of the naturally weighted beam is still dictated by the size of the outer ring. Small differences among different arrays exist because of varying topographical and other limitations.

The Kogan optimization was performed allowing the pad positions to drift *anywhere within the annular region defined by the two circles*, but the

sidelobe optimization generally pushes all of the antennas to the boundaries of the allowed region, arranging all pads to be located along the inner and the outer circle. The array design was done outside in, starting with the A-array. The pad positions along the inner ring of the A-array are held fixed to derive the remaining 32 pad positions for the B-array, and this process was repeated until the inner ring of the D-array was found (which is the outer boundary ring of the E-array). The pad locations and the resulting snapshot uv-coverage and dirty beams for the C-array are shown in Figure 2 as an example.

3.3 3km Array (A-array)

The layout of the 3km array is essentially the same as the intermediate arrays discussed above. An important additional concern is that the topographic restrictions are severe for an array this large, and few suitable locations exist within the Science Reserve boundary. Once chosen, the center of the 3km array defines the center of all other arrays, as shown schematically in the top left panel of Figure 3. The chosen center does not coincide with any of the three candidate compact array sites identified from the digital elevation model during the site visit in November 1999 (shown as large circles in Fig. 3), but it is within a few hundred meters of the “Chajnantor South” position.

Because of its large size, the shortest baseline present in the current strawperson design is 85m. This should not pose a problem for imaging compact sources, but adding data from a smaller configuration may be needed when mapping extended sources (see below). This may be avoided by incorporating a compact cluster of 3-4 antennas without greatly impacting the high angular resolution performance.

A snapshot uv-coverage from this array covers less than 1% of all uv cells, and a full earth synthesis lasting more than 6 hrs may be needed for good imaging performance (fraction of occupied cells $FOC \geq 0.3$). The maximum near-in sidelobe is only about 4%. Larger sidelobes are present in the outer regions of the snapshot dirty beam, but they are quickly reduced to less than 2% with some earth rotation synthesis.

4 Imaging Performance

As shown in Figure 4 (also see Table 1), 40% or more of the uv cells can be sampled nearly instantaneously for the two smallest configurations and in less than 2 hrs for the C-array. It takes about 4 hrs for the second largest configuration, and only the 3km array requires a full synthesis lasting more than 6 hrs to sample a substantial fraction of the uv cells.

An extensive program to examine the imaging performances of the competing strawperson arrays, is currently underway by S. Heddle and others. Several simulated observations of Cygnus A are shown in Figures 5-7, simply as a demonstration of the imaging performance by our strawperson arrays. The model image used is the VLA multi-configuration map of Cygnus-A kindly provided to us by C. Carilli and R. Perley. This model image is scaled down to have a total linear extent of $10''$, which is about 1/2 of the primary beam ($18''.35$ at 345 GHz). The simulated observation with the compact array reproduces the expected source brightness distribution quite well, even in a snapshot (see Figure 5). The imaging performance is also excellent for the 4 hr long observations in the C-array (Figure 6).

As mentioned earlier, the simulated observation by the 3km configuration alone suffers greatly from missing short spacing information and poorly reproduces the extended radio lobes in Cygnus A (see the top panel in Figure 7). This is a direct consequence of the fact that the shortest baseline in the 3km array is 85m long – the largest structure the A-array is sensitive to is about $2''$ at 345 GHz. When 15 minute snapshot data from the C-array is added, the representation of the extended structures is significantly improved (see the bottom panel in Figure 7). Therefore, multi-configuration observation may not be avoidable in some imaging projects in the largest configuration, but this may be accomplished successfully with the existing sets of strawperson configurations as demonstrated here.

5 Summary and Discussion

The donut/double-ring strawperson configurations presented here retain the fast and uniform uv sampling capability of a ring array while significantly reducing the near-in sidelobe level to below 4-5% level using a double ring design and Kogan sidelobe minimization algorithm. The claimed improvements are demonstrated by the uv-coverage and simulated observations of an astronomical source.

Some room for improvement exists, however. Missing short baselines for the A-array clearly poses a problem for imaging sources larger than about $1/7$ of the primary beam. This problem may be addressed with a further modification of the pad layout, but the problem may be more fundamental in nature, requiring a more concrete solution such as accepting multi-configuration synthesis as a standard observing mode.

The near-in sidelobes are already reasonably low at 4-5%, but an even lower level may benefit the deconvolution process. In the zoom spiral design, this is accomplished by heavily over-sampling the core of the uv distribution and sparsely sampling the outer uv-plane. Because sources to be studied with ALMA are expected to possess complex structures in general, the quality of the produced image may be determined by the completeness of the sampling in the uv-plane (e.g. Woody 1999), and whether the sacrifice in the uv sampling efficiency is justifiable has to be addressed. Existing image reconstruction algorithms in use are developed for sparsely sampled data, and new algorithms taking full advantage of the complete Fourier plane sampling should be investigated regardless.

The antenna transport times and reconfiguration memo by Radford (1999) can be consulted directly for the reconfiguration of these strawperson arrays. Radford estimates that an array such as this can be reconfigured in just 2-3 days even under the most pessimistic assumptions (see his Figure 2, but this is $1/2$ of the duration computed by Radford since the current design requires moving only one half of all antennas for a reconfiguration). Hybrid configurations with N-S elongation of 2:1 are highly desirable for imaging objects transiting at low elevations. A reconfiguration into such a hybrid array can be accomplished by moving just 16 antennas, requiring only a little over a day (and requiring only one additional day or so to complete the entire reconfiguration into the next array). Two full configuration cycles per year would be ideal so that every object in the sky can be observed during night time in each configuration at some point during the year. The 10+ km array will require at least 2 weeks of time just for reconfiguration, and it should be scheduled at most once a year. Under such a reconfiguration plan, the array will stay in each configuration for about 4 weeks, long enough to outlast most adverse weather patterns or extended holidays and to accomplish most of the observations requiring the specific resolution. Unlike the continuous reconfiguration mode, the full complement of 64 antennas will be available for observations nearly all of the time.

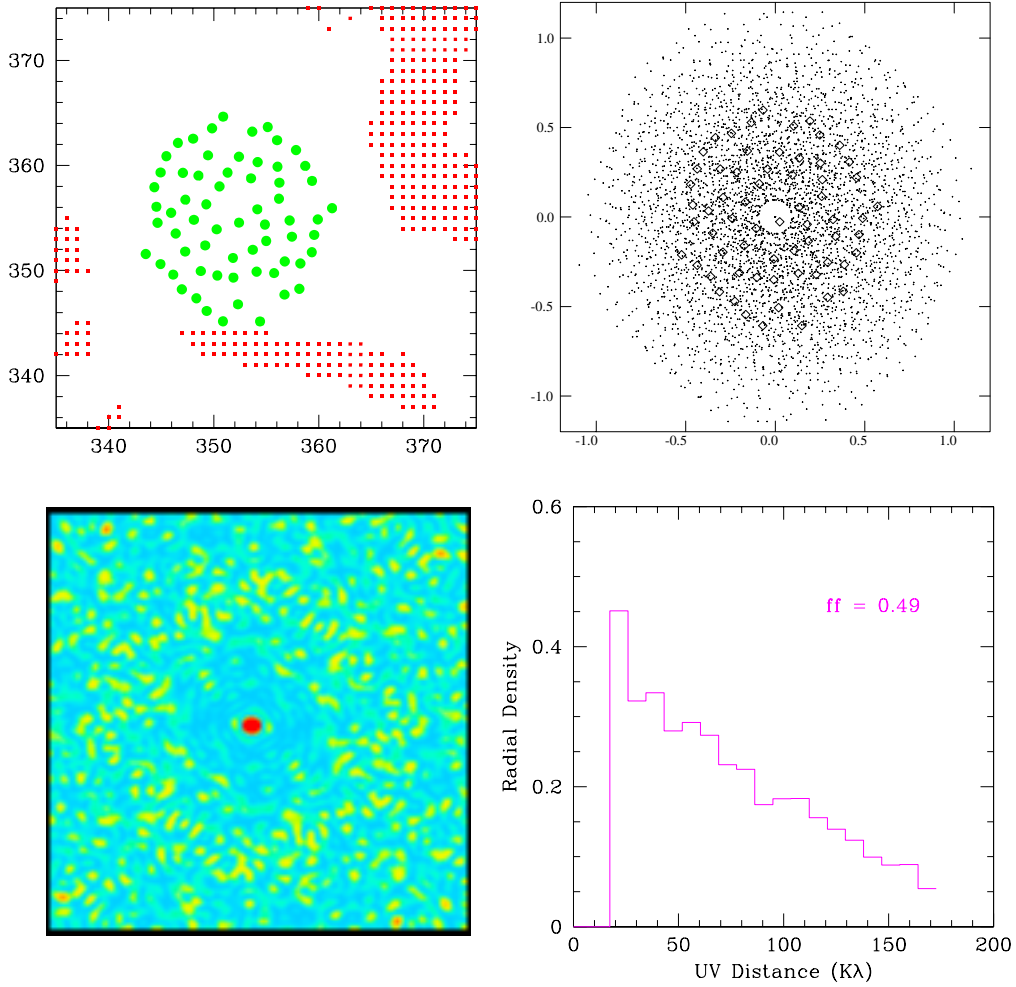


Figure 1: (Upper Left) Pad positions for the E-array shown in filled circles. The x- and y-axis represent the pixel position in topographical mask, where one pixel is 10 meter in size. The shaded areas mark the forbidden zones in the topographical mask. (Upper Right) Snapshot uv-coverage from CONF1. (Lower Left) Naturally weighted snapshot dirty beam. The plotted color ranges between -5% and $+10\%$. The maximum near-in sidelobe is about 4%, and the largest sidelobe with the PB is about 10%. (Lower Right) Radial density distribution of the visibilities. Nearly 50% of the uv cells are sampled instantaneously.

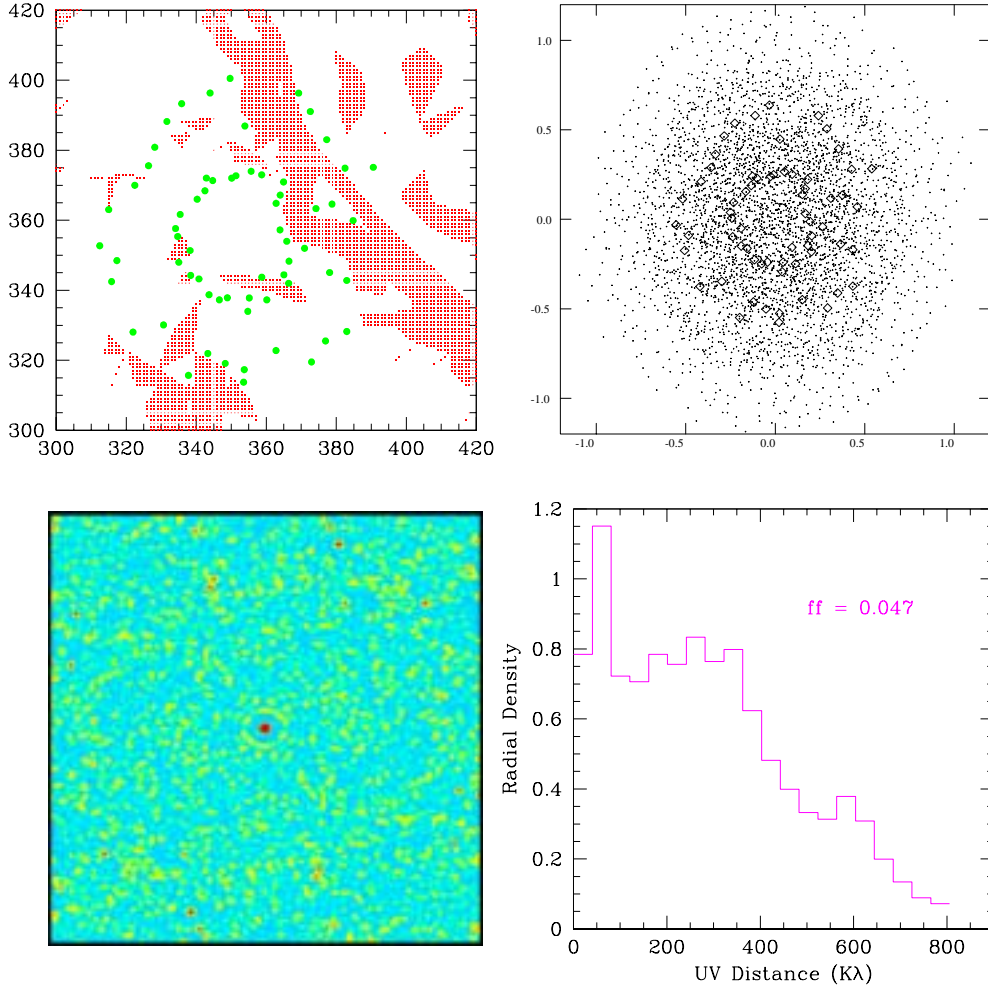


Figure 2: (Upper Left) Pad positions for the C-array shown in filled circles. The shaded areas marks the forbidden zones in the topographical mask. (Upper Right) Snapshot uv-coverage from CONF1. (Lower Left) Naturally weighted snapshot dirty beam. The plotted color ranges between -5% and $+10\%$. The maximum near-in sidelobe is about 5% . (Lower Right) Radial density distribution of the visibilities. Only 5% of the uv cells are sampled instantaneously, but up to 40% of the cells can be sampled after 90 minutes of observations (see Table 1).

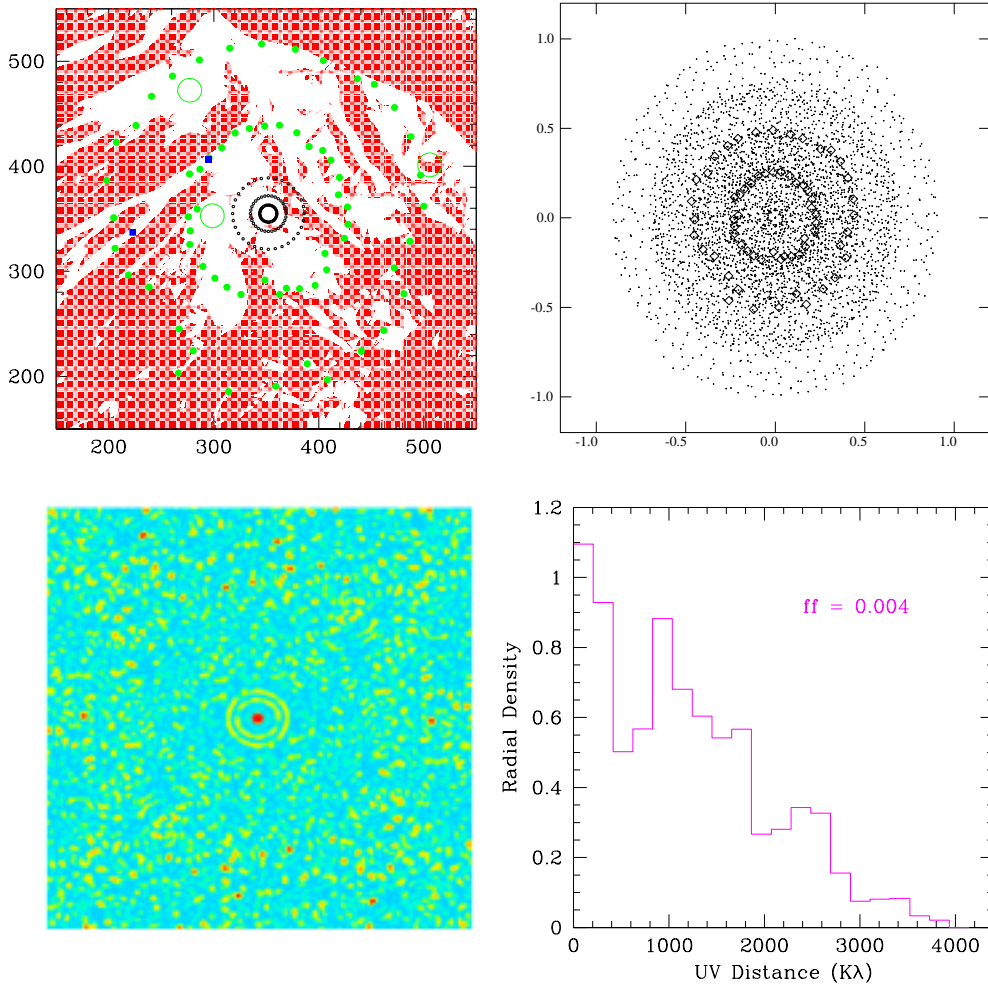


Figure 3: (Upper Left) Pad positions for the A-array are shown in filled circles. The two small squares mark the current positions of the NRAO and ESO site testing equipment containers. The three other configurations are also shown schematically as nested rings. The shaded areas marks the forbidden zones in the topographical mask. (Upper Right) Snapshot uv-coverage from CONF1. (Lower Left) Naturally weighted snapshot dirty beam. The plotted color ranges between -5% and $+10\%$. The maximum near-in sidelobe is about 4% . The outer sidelobes are suppressed below 1.5% when a full earth rotation synthesis is performed. (Lower Right) Radial density distribution of the visibilities. Only 0.4% of the uv cells are sampled instantaneously, and a full 10 hr earth rotation synthesis is needed to sample up to 40% of uv cells.

Fraction of Occupied Cells

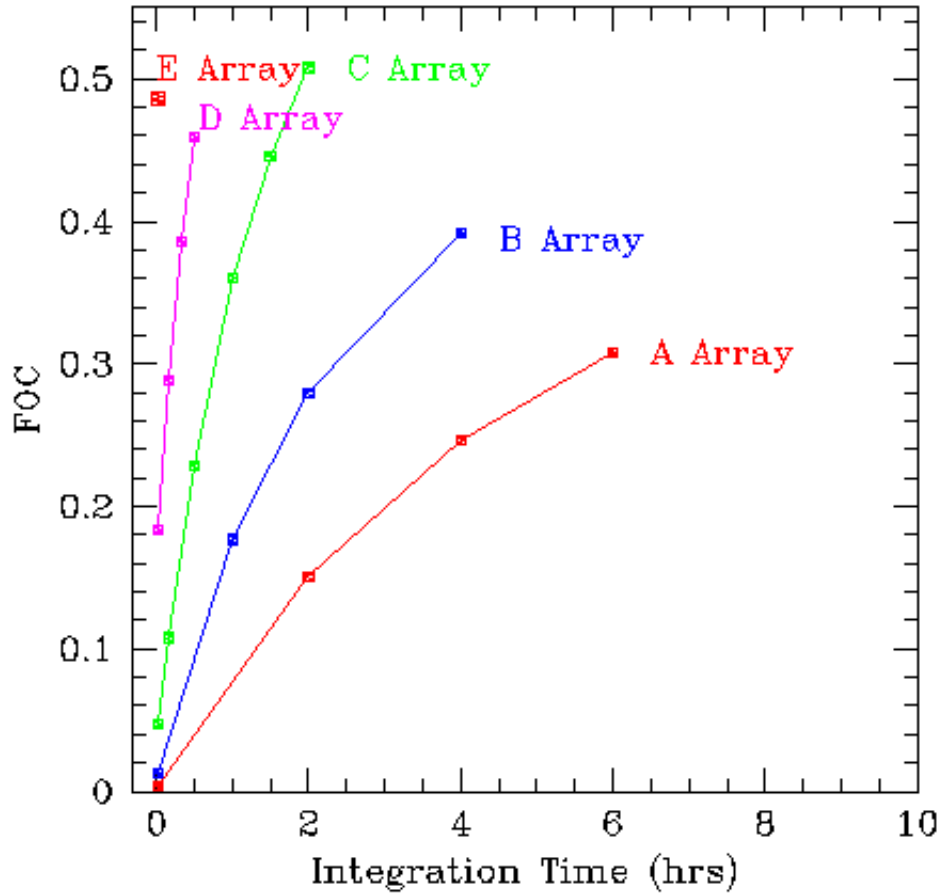


Figure 4: Fraction of the uv cells sampled by each configuration with earth rotation synthesis. For a good imaging performance, sampling 40% or more of the uv cells may be needed.

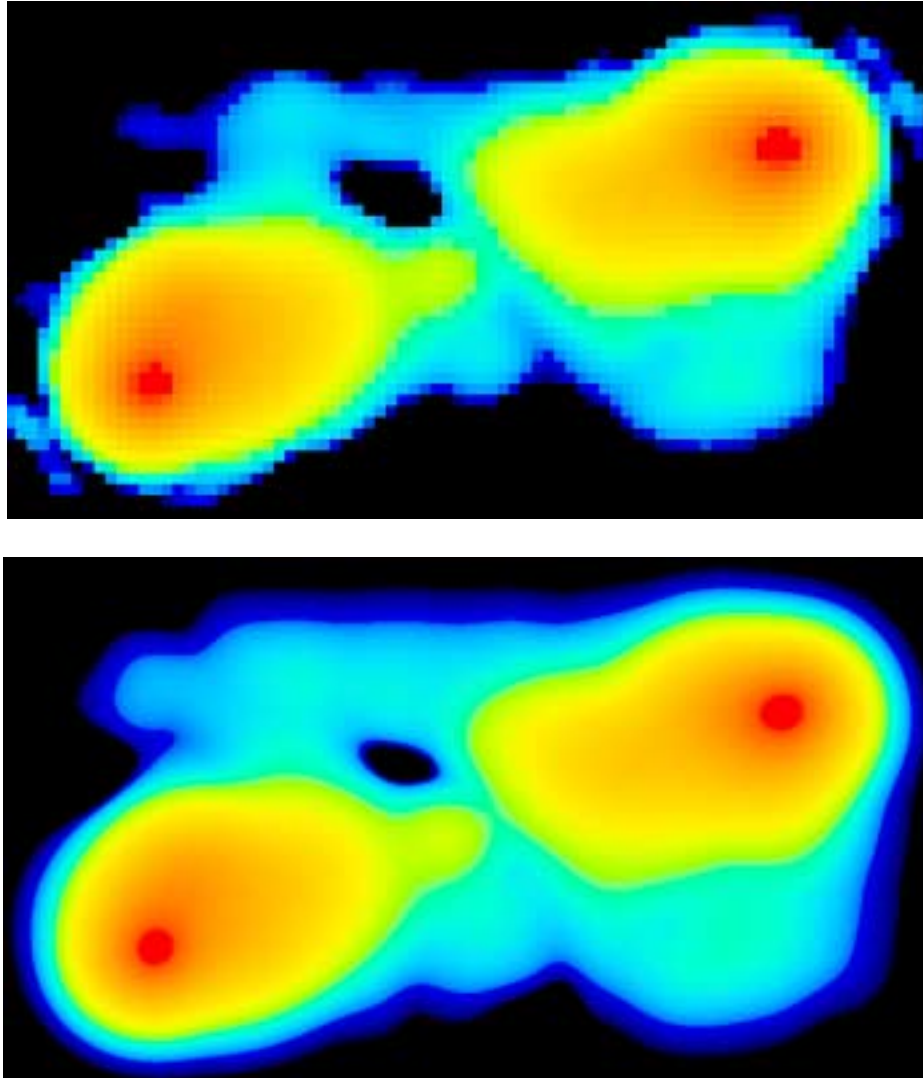


Figure 5: (Top) A simulated observation of Cygnus A from the snapshot observation in the compact array at $1''$ resolution at 345 GHz (restored with CLEAN). The images are displayed in logarithmic scales to show details at faint levels. The total extent of the input model source is about $10''$, which is about $1/2$ of the primary beam of the 12m antenna at 345 GHz. (Bottom) A corresponding model image obtained by convolving the input model image with a $1''$ diameter Gaussian beam.

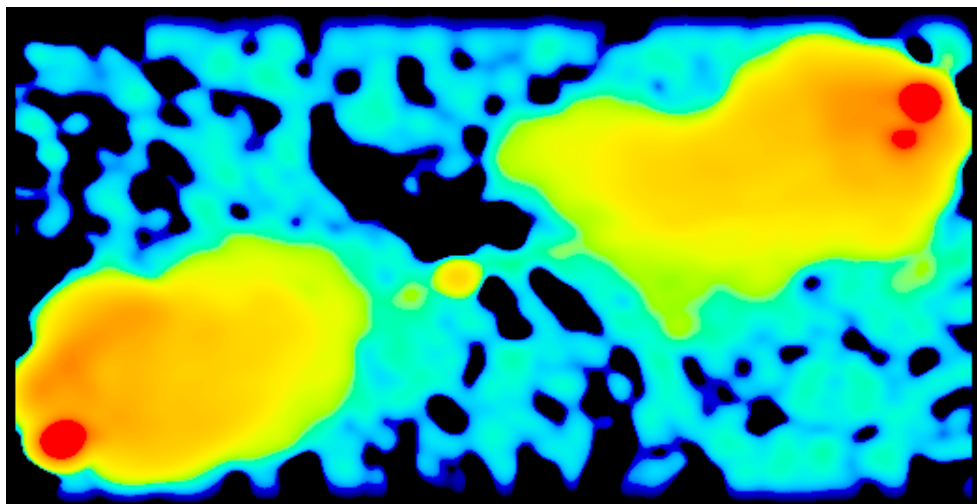
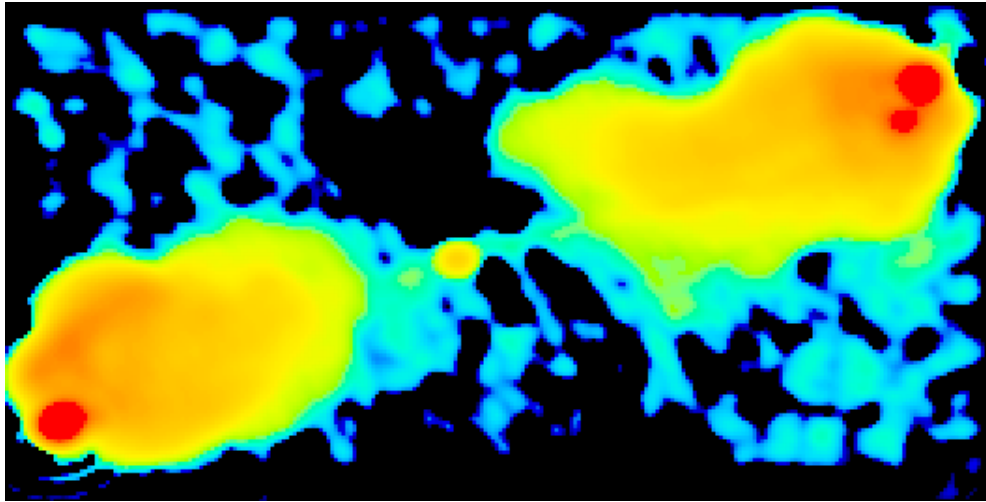


Figure 6: (Top) A simulated observation of Cygnus A from the 4 hr long earth rotation synthesis in the C-array. (Bottom) A corresponding model image obtained by convolving the input model image with a $0.22''$ diameter Gaussian beam.

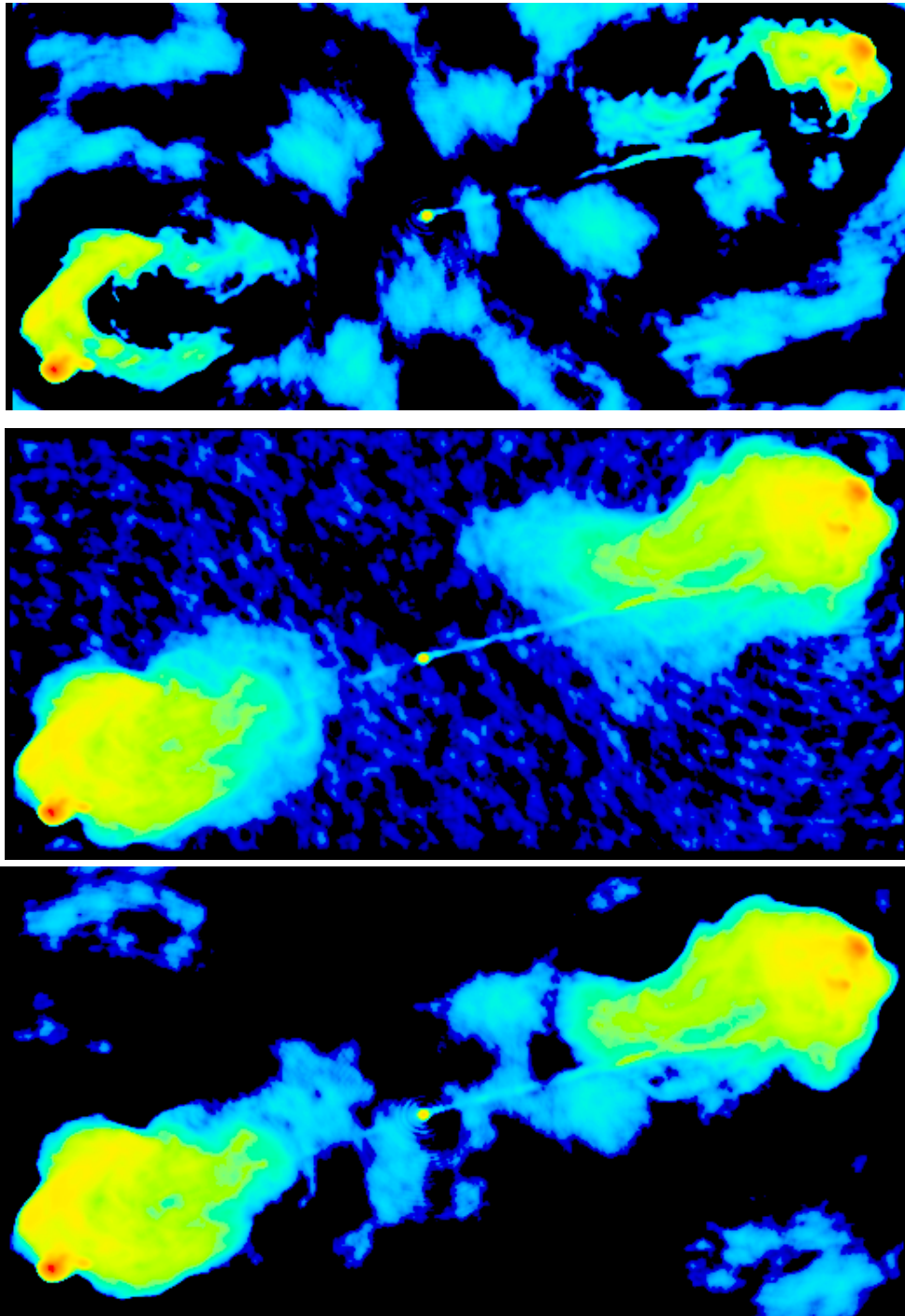


Figure 7: (Top) A simulated observation of Cygnus A from the 4 hr long earth rotation synthesis in the A-array. (Middle) A corresponding model image obtained by convolving the input model image with a Gaussian beam with $0.05''$ in diameter. (Bottom) A simulated 4 hr long earth rotation synthesis in the A-array plus a 15 minute long snapshot data from the C-array.

REFERENCES

- Conway, J. 1998, "Self-Similar Spiral Geometries for the LSA/MMA," MMA Memo No. 216
- Conway, J. 2000a, "Observing Efficiency of a Strawperson Zoom Array," ALMA Memo 283.
- Conway, J. 2000b, "A Possible Layout for a Spiral Zoom Array Incorporating Terrain Constraints," ALMA Memo 292.
- Guilloteau, S. 1999, "Reconfiguring the ALMA Array", ALMA Memo 274.
- Helfer, T., & Holdaway, M. 1998, "Design Concepts for Strawperson Antenna Configurations for the MMA," MMA Memo 198
- Holdaway, M. 1994, "Preliminary MMA Configurations for Mauna Kea," MMA Memo No. 111
- Holdaway, M. 1998a, "Cost-Benefit Analysis for the Number of MMA Configurations," MMA Memo No. 199
- Holdaway, M. 1998b, "Hour Angle Ranges for Configuration Optimization," MMA Memo No. 201
- Keto, E. 1997, "The Shapes of Cross-Correlation Interferometers," ApJ, 475, 843
- Kogan, L. 1998a, "Optimization of an Array Configuration with a Donut Constraint", MMA Memo No. 212
- Kogan, L. 1998b, "A, B, C, and D configurations in the shape of concentric circles with fixed pads at the common circumferences", MMA Memo No. 226
- Radford, S. J. E. 1999, "Antenna Transport Times and Reconfiguration Schedule," ALMA Memo No. 280.
- Woody, D. 1999, "ALMA Configurations with Complete UV Coverage," ALMA Memo No. 270.
- Yun, M., & Kogan, L. 1999, " Cost-Benefit Analysis of ALMA Configurations," ALMA Memo No. 265.